# Effect of Neutrals on Scrape-Off-Layer and Divertor Stability in Tokamaks

D. A. D'Ippolito† and J. R. Myra

*Lodestar Research Corporation,*
*2400 Central Avenue,*
*Boulder, Colorado 80301*

Abstract

The influence of ion-neutral interactions (charge exchange, elastic scattering) on scrape-off-layer (SOL) stability is studied in the eikonal limit for a single-null X-point geometry typical of tokamak divertors. Instability drives due to curvature and to the ion-neutral drag effect are included in the model. The ion-neutral interaction terms are highly localized near the divertor plates; these terms are stabilizing for typical parameters and large enough to affect the SOL ballooning-interchange stability in the absence of resistivity. It is shown that the growth rate of ideal curvature-driven modes is significantly reduced by the ion-neutral interaction terms; the growth rate of resistive ballooning modes is not affected much by the neutrals, because resistivity allows the mode to disconnect from the divertor region. In both cases, the X-point geometry significantly affects the stability. An ion-neutral drag instability localized near the plates is only found in a small region of parameter space. Conditions for the existence of this instability in X-point geometry are discussed.

PACS numbers: 52.35.Py, 52.25.Ya, 52.30.Jb, 52.55.Fa

†email: dasd@lodestar.com

## I. Introduction

Neutral particles play an important role in the equilibrium and energy balance of tokamak divertor plasmas. Neutrals and ions are coupled by the processes of charge exchange, ionization and recombination. This coupling is illustrated in a striking way by the phenomenon of detached divertor plasmas, in which the plasma density, temperature and pressure are quenched at some distance from the divertor plates by the interaction with neutral particles.

Recent work suggests that ion-neutral interactions can also influence the magnetohydrodynamic (MHD) stability of interchange-ballooning modes in the scrape-off-layer (SOL) and divertor plasmas.[1-3] Elastic collisions and charge exchange between the ion and neutral fluids introduce an effective frictional force $\mathbf{f} = -\nu(\mathbf{u} - \mathbf{u}_0) = -\nabla p_0/\rho$, where the latter form of $\mathbf{f}$ follows from the equilibrium pressure balance relation. Here, the subscript 0 denotes neutral quantities, $\nu$ is the frequency of ion-neutral "collisions" (typically dominated by charge exchange), $(\mathbf{u} - \mathbf{u}_0)$ denotes the relative speed of the ion and neutral fluids, $\rho$ is the plasma mass density, and $p_0$ is the neutral pressure. This frictional force yields both a stabilizing collisional damping of MHD modes and a new source of instability. This is illustrated by the following dispersion relation:

$$\omega^2 - \langle f_\eta k_\parallel^2 v_a^2 \rangle + i\langle\nu\rangle\omega + \langle\gamma_\kappa^2 + \gamma_\nu^2\rangle = 0 , \tag{1a}$$

$$\gamma_\kappa^2 \equiv \frac{8\pi v_a^2}{k_\perp^2 B^2} \mathbf{k}\times\mathbf{b}\cdot\nabla p \;\; \mathbf{k}\times\mathbf{b}\cdot\boldsymbol{\kappa} , \tag{1b}$$

$$\gamma_\nu^2 \equiv \frac{\nu}{k_\perp^2} \mathbf{k}\times\mathbf{b}\cdot\nabla \ln\rho \;\; \mathbf{k}\times\mathbf{b}\cdot(\mathbf{u} - \mathbf{u}_0) ,$$

$$= \frac{1}{\rho\, k_\perp^2} \mathbf{k}\times\mathbf{b}\cdot\nabla \ln\rho \;\; \mathbf{k}\times\mathbf{b}\cdot\nabla p_0 , \tag{1c}$$

where $\omega$ is the MHD mode frequency, $f_\eta = \omega/(\omega + \omega_\eta)$ and $\omega_\eta = i\,\eta\,k_\perp^2 c^2/4\pi$. The angular brackets denote the appropriate field line average, $\langle Q\rangle = \int ds\, w\, |\tilde{\phi}|^2\, Q \,/\, \int ds\, w\, |\tilde{\phi}|^2$, where s is the arclength along the B field, $w = k_\perp^2 / v_a^2$ is the appropriate weighting function, and $\tilde{\phi}$ is the eigenfunction ($\tilde{\phi}$ = constant in the $k_\parallel = 0$ interchange limit). The terms in Eq. (1a) describe the plasma inertia, the magnetic field line bending energy (including the effect of resistivity), the ion-neutral collisional dissipation, the curvature-drive term, and the ion-neutral drag instability[4-5] drive term.

In the "unperturbed neutral" limit (where the neutral density, temperature and velocity are regarded as unperturbed by the mode), the neutral instability drive is analogous to the gravitational instability with the effective gravity replaced by $\mathbf{f}$. Taking into account the charge separation induced by the $\mathbf{f} \times \mathbf{b}$ drift, one finds that an initial density perturbation will grow if the condition $\mathbf{k} \times \mathbf{b} \cdot \nabla \ln \rho \;\; \mathbf{k} \times \mathbf{b} \cdot \mathbf{f} \; < 0$ is satisfied, which implies $\gamma_\nu^2 > 0$ in Eq. (1). Thus, the condition for instability imposes the restriction that the plasma density and neutral pressure gradients have components in the same direction. More rigorous stability calculations (see Ref. 1 and Sec. II) verify this simple physical picture.

Recently, several aspects of the ion-neutral drag instability have been investigated in order to understand its relevance to SOL and divertor plasma stability. The linear interchange stability picture has been discussed in slab geometry for both the unperturbed and perturbed neutral regimes.[1] In this work, a fluid treatment was given for the small mean-free-path limit and a kinetic treatment was used for the long mean-free-path neutral regime. Other work using a fluid treatment in more realistic X-point geometry[2] suggested that the ion-neutral drag instability might have a significant growth rate when the dominant ion density and neutral pressure gradients are in the same direction. Finally, a

simulation of the nonlinear phase, again in slab geometry, concluded that the saturation levels of the mode could be substantial.[3]

Two aspects of the problem require further treatment in order to draw conclusions about the relevance of this instability to realistic tokamak plasmas. First, the stability picture was shown to be extremely sensitive to the details of a model X-point geometry and to the assumed plasma and neutral profiles.[2] Second, the localization of the neutrals to the divertor region implies that the influence of the ion-neutral friction on extended MHD (ballooning) modes must be determined by a self-consistent numerical solution including the other important terms in the ballooning equation (line-tying, line-bending, resistivity, etc.). The sensitivity of the growth rate to the eigenfunction weighting is evident from Eq. (1).

The present paper extends previous work on ion-neutral stability physics by carrying out numerical solutions of the ballooning equation for a model X-point geometry (using the techniques of Ref. 6) with plasma and neutral profiles that qualitatively describe high-recycling and detached divertor plasmas. Our numerical survey shows that the condition for the ion-neutral drag instability is typically not satisfied for realistic equilibria. In two of the cases studied (high-recycling and completely detached plasmas), the instability drive for interchange-ballooning modes is the usual curvature drive, the $\gamma_\nu^2$ term is stabilizing, and the friction term $i\nu\omega$ also contributes to a reduction in the growth rate. In the limit of negligible resistivity, relevant to modes with very low n (toroidal mode number), the neutral terms can have a significant stabilizing effect. In the resistive limit, relevant to high-n modes, the most unstable eigenmode decouples from the divertor regions and the effect of the neutrals on the instability disappears. The resistivity also permits an instability branch localized in the divertor region and driven by $\gamma_\nu^2$. This branch has also been found numerically for a “semi-detached” equilibrium (described in

Sec. IV) which satisfies the analytic instability condition but may not be physically consistent.

The plan of this paper is as follows. In Sec. II we derive the general fluid stability expression retaining neutral perturbations. Although an accurate treatment of the neutral perturbations can only be done kinetically,[1] the fluid derivation allows us to show that the relevant coupling parameter is $\Lambda = i\rho\nu / (i\rho\nu + \rho_0 \tilde{\omega}_0 + i\rho_0 k_\perp^2 D_0)$, where $\tilde{\omega}_0 = \omega - \mathbf{k} \cdot \mathbf{u}_0$ and $D_0$ is the neutral viscous diffusion coefficient defined in Sec. II. The "unperturbed neutral" fluid model is valid in the limit $\Lambda << 1$, and we derive a ballooning equation in this limit which incorporates both the effect of neutrals and of plasma resistivity. In Sec. III, our equilibrium model is described, consisting of a "two-wire" model for the X-point geometry and analytic plasma and neutral profiles for a variety of divertor plasma regimes. In Sec. IV, the numerical results are described and a brief survey of the relevant parameter space is given. A summary and discussion is given in Sec. V.

## II. Basic Equations

In this section, we summarize the derivation of the neutral-drag contribution to the ballooning equation including the neutral perturbation terms ( $\tilde{u}_0$ , $\tilde{\rho}_0 \neq 0$). Although a kinetic treatment[1] is needed to describe neutral perturbations in the limit of long-mean-free-path neutrals, a fluid model is adequate to describe the high-neutral-density divertor regimes of most interest for the ion-neutral drag instability.

The starting point of the calculation is the following set of plasma and neutral fluid equations:

$$\frac{\partial \rho}{\partial t} + \nabla \cdot (\rho \mathbf{u}) = 0, \tag{2}$$

$$\frac{\partial \rho_0}{\partial t} + \nabla \cdot (\rho_0 \mathbf{u}_0) = 0, \tag{3}$$

$$\rho \frac{d\mathbf{u}}{dt} - \frac{1}{c} \mathbf{J} \times \mathbf{B} + \nabla p + \rho\nu(\mathbf{u} - \mathbf{u}_0) = 0, \tag{4}$$

$$\rho_0 \frac{d\mathbf{u}_0}{dt} + \nabla p_0 - \rho\nu(\mathbf{u} - \mathbf{u}_0) - \rho_0 D_0 \nabla^2 \mathbf{u}_0 = 0 \quad , \tag{5}$$

$$\mathbf{E} + \frac{1}{c}\mathbf{u} \times \mathbf{B} - \eta\, J_{\parallel}\, \mathbf{b} = 0, \tag{6}$$

$$\nabla \cdot \mathbf{J} = 0. \tag{7}$$

Equations (4) and (6) can be solved for $\mathbf{J}_\perp$ and $\mathbf{u}_\perp$ to obtain:

$$\mathbf{u}_\perp = -\mathbf{b} \times \frac{c}{B}\mathbf{E} \, , \tag{8}$$

$$\mathbf{J}_\perp = \frac{c}{B}\mathbf{b} \times \{ \nabla p + \rho\nu(\mathbf{u} - \mathbf{u}_0) + \rho \frac{d\mathbf{u}}{dt} \} . \tag{9}$$

Note that the subscript 0 is used here to denote neutral quantities, not equilibrium values. Here, $\rho = m_i n_i + m_e n_e$ and $\rho_0 = m_0 n_0$ are the plasma and neutral mass densities, $\mathbf{u}$ and $\mathbf{u}_0$ are the plasma and neutral fluid velocities, $\mathbf{E}$ and $\mathbf{B} = B\mathbf{b}$ are the electric and magnetic fields, $\mathbf{J}$ is the plasma current, $p = p_i + p_e$ and $p_0$ are the plasma and neutral fluid pressures, $\Omega_i = (eB/m_i c)$ is the ion cyclotron frequency and $\eta$ is the parallel resistivity. Following Daughton et al.[1] a simplified form of the neutral viscosity is introduced into the neutral momentum equation, Eq. (5), where the neutral viscous diffusion coefficient is defined by $D_0 = v_0^2/(2\nu_0)$ and $v_0$ is the neutral thermal speed. The collision frequencies are defined as follows: $\nu \equiv n_0 \langle\sigma v\rangle_{in}$ and $\nu_0 \equiv n_i \langle\sigma v\rangle_{in} = (\rho/\rho_0)\,\nu$ are the ion-neutral and neutral-ion collision frequencies, respectively. The form of viscosity used here is valid in the collisional limit ($d/dt,\ k_\perp^2 D_0 << \nu_0$) as discussed in Ref. 1. In the numerical work to follow, we use the approximate formula $\langle\sigma v\rangle_{in} = \sigma_{in} v_i$, where $v_i$ is the ion thermal velocity and the cross-section for charge exchange is given by $\sigma_{in} \approx 5 \times 10^{-15}$ $cm^2$.

It follows from this system of equations that the plasma-neutral equilibrium is given by

$$\nabla p_0 = \rho\nu(\mathbf{u} - \mathbf{u}_0) \, , \tag{10}$$

$$\mathbf{u}_\perp = -\mathbf{b} \times \frac{c}{B}\mathbf{E} \, , \tag{11}$$

$$\mathbf{J}_\perp = \frac{c}{B}\mathbf{b}\times\{\nabla p + \rho\nu(\mathbf{u}-\mathbf{u}_0)\}, \tag{12}$$

where the equilibrium viscosity term is assumed to be negligible.

To simplify the derivation of the stability equations, we make the low-frequency approximation $\omega, \nu << \Omega_i$. The generalization to finite $\omega/\Omega_i$ is straightforward but tedious and adds little physical insight. We also use straight magnetic field lines in the derivation of the neutral stability terms and add the curvature drive term back into the final result. The ballooning equation is derived from the linearized version of Eq. (7) with the perturbation of a quantity Q varying as $\tilde{Q} \propto \exp[\mathbf{k}\cdot\mathbf{x} - \omega t]$. In the eikonal limit ($k_\perp L >> 1$, where L is any equilibrium gradient length) the following result for $\nabla\cdot\mathbf{J}_\perp$ is obtained

$$\nabla\cdot\mathbf{J}_\perp = -\frac{c}{B}\mathbf{b}\cdot\nabla\times\{\rho\frac{d\mathbf{u}}{dt} + \rho\nu(\mathbf{u}-\mathbf{u}_0)\}. \tag{13}$$

We linearize Eq. (13) in the electrostatic approximation ($\tilde{B} = \tilde{\mathbf{b}} = 0$). Neglecting higher order terms in the eikonal approximation, we obtain

$$\nabla\cdot\tilde{\mathbf{J}}_\perp = \frac{c}{B}\Big\{\rho(\tilde{\omega}+i\nu)\,\mathbf{k}\times\mathbf{b}\cdot\tilde{\mathbf{u}} + i\rho(\tilde{\omega}+i\nu)\,\mathbf{b}\times\nabla\rho\cdot\tilde{\mathbf{u}}$$

$$+ i\rho\nu\,\mathbf{k}\times\mathbf{b}\cdot(\mathbf{u}-\mathbf{u}_0)\left(\frac{\tilde{\rho}}{\rho} + \frac{\tilde{\rho}_0}{\rho_0}\right) - i\rho\nu\,\mathbf{k}\times\mathbf{b}\cdot\tilde{\mathbf{u}}_0\Big\}, \tag{14}$$

where $\tilde{\omega} = \omega - \mathbf{k}\cdot\mathbf{u}$ is the Doppler-shifted frequency in the plasma rest frame. At this point we introduce the notation

$$\tilde{\mathbf{u}} = \frac{X}{k^2}\mathbf{k} + \frac{Y}{k^2}\mathbf{k}\times\mathbf{b}, \tag{15}$$

$$\tilde{\mathbf{u}}_0 = \frac{X_0}{k^2}\mathbf{k} + \frac{Y_0}{k^2}\mathbf{k}\times\mathbf{b}, \tag{16}$$

with $X \equiv \mathbf{k}\cdot\tilde{\mathbf{u}}$ $Y \equiv \mathbf{k}\times\mathbf{b}\cdot\tilde{\mathbf{u}}$ $X_0 \equiv \mathbf{k}\cdot\tilde{\mathbf{u}}_0$ and $Y_0 \equiv \mathbf{k}\times\mathbf{b}\cdot\tilde{\mathbf{u}}_0$. The linearized versions of Eqs. (2) and (3) can then be written in the form

$$\frac{\tilde{\rho}}{\rho} = \frac{1}{\tilde{\omega}}\left(X - \frac{iY}{k^2}\mathbf{k}\times\mathbf{b}\cdot\nabla\ln\rho\right), \tag{17}$$

$$\frac{\tilde{\rho}_0}{\rho_0} = \frac{1}{\tilde{\omega}_0}\left(X_0 - \frac{iY_0}{k^2}\mathbf{k}\times\mathbf{b}\cdot\nabla\ln\rho_0\right), \tag{18}$$

where again higher-order terms in the eikonal approximation have been omitted and the definition $\tilde{\omega}_0 \equiv \omega - \mathbf{k}\cdot\mathbf{u}_0$ is introduced. The perturbed electric field is given by

$$\tilde{\mathbf{E}} = -\nabla\tilde{\phi} - \frac{1}{c}\frac{\partial}{\partial t}\tilde{\mathbf{A}} , \tag{19}$$

where $\tilde{\mathbf{A}}_\perp$ vanishes in lowest order for the incompressible ($\nabla\cdot\mathbf{u} = 0$) interchange-ballooning modes of interest here. Thus, in the low-frequency limit Eq. (11) yields

$$X = 0 , \qquad Y = -\frac{ick_\perp^2}{B}\tilde{\phi} . \tag{20}$$

The solution of the linearized Eq. (5) for $\tilde{\mathbf{u}}_0$ employing Eqs. (15) - (18) implies

$$X_0 = \frac{\Lambda}{\Upsilon}\left\{ X + \mathbf{k}\cdot(\mathbf{u}-\mathbf{u}_0)\frac{\tilde{\rho}}{\rho} - i\frac{k_\perp^2 v_0^2}{\nu_0}\frac{\tilde{\rho}_0}{\rho_0}\right\} , \tag{21a}$$

$$Y_0 = \frac{\Lambda}{\Upsilon}\left\{ Y + \mathbf{k}\times\mathbf{b}\cdot(\mathbf{u}-\mathbf{u}_0)\frac{\tilde{\rho}}{\rho}\right\} , \tag{21b}$$

$$\Lambda = \frac{i\rho\nu}{i\rho\nu + \rho_0\tilde{\omega}_0 + i\rho_0 k_\perp^2 D_0} = \frac{i\nu_0}{i\nu_0 + \tilde{\omega}_0 + i k_\perp^2 D_0} , \tag{21c}$$

where $\Upsilon = 1 + i\,\alpha\Lambda$, $\alpha \equiv (k_\perp^2 v_0^2/\omega\nu_0) = (k_\perp^2\lambda_0^2)(\nu_0/\omega)$ and $\lambda_0 = v_0/\nu_0$ is the neutral mean-free-path. In linearizing Eq. (5) to obtain Eq. (21), we have neglected the neutral temperature perturbation ($\tilde{T}_0 = 0$) and have used the equilibrium relation $p_0 = \rho_0 v_0^2$. From Eqs. (18) and (21) we note that the perturbed neutral quantities $\tilde{\rho}_0$ and $\tilde{\mathbf{u}}_0$ are proportional to $\Lambda$, so that this is the desired coupling parameter ($0 < \Lambda < 1$) for neutral perturbation physics. The effect of neutral viscosity is contained in $\Lambda$ and the perturbed pressure term ($\propto \alpha$) enters in the coefficient $\Upsilon$.

Finally, combining Eqs. (14) - (21), making use of the approximation $k_\perp L >> 1$, and adding back the curvature drive term $\gamma_\kappa^2$, we obtain:

$$\nabla\cdot\tilde{\mathbf{J}}_\perp = \frac{c\rho Y}{B\tilde{\omega}}\left\{\tilde{\omega}^2 + \gamma_\kappa^2 + (1-\Lambda)(i\nu\tilde{\omega} + \gamma_\nu^2)\right.$$

$$\left. + \frac{\Lambda\gamma_\nu^2}{\Upsilon}\left[\frac{\mathbf{k}\cdot(\mathbf{u}-\mathbf{u}_0)}{\tilde{\omega}_0} + \frac{L_{ni}}{L_{n0}}\frac{\tilde{\omega}}{\tilde{\omega}_0}\right]\right\} , \tag{22a}$$

where the drive terms for the magnetic curvature- and neutral collision-driven instabilities are defined in Eq. (1) and the radial scale lengths $L_{ni}$ and $L_{n0}$ in Eq. (22) are given by

$$L_{ni}^{-1} = \mathbf{k} \times \mathbf{b} \cdot \boldsymbol{\nabla} \ln \rho \,, \tag{22b}$$

$$L_{n0}^{-1} = \mathbf{k} \times \mathbf{b} \cdot \boldsymbol{\nabla} \ln \rho_0 \,. \tag{22c}$$

The first two terms in Eq. (22a) are the plasma inertia and curvature-drive terms. The quantity $\gamma_\nu^2$ is the square of the growth rate of the ion-neutral drag instability in the unperturbed neutral limit ($\Lambda \to 0$), as obtained in the early calculations.[4,5] The terms proportional to $\Lambda$ represent the effects of the neutral perturbations in the fluid model; specifically, the terms in Eq. (22a) with $\Lambda$ and $\Lambda/\Upsilon$ arise from the terms proportional to $\tilde{\mathbf{u}}_0$ and $\tilde{\rho}_0$, respectively, in $\nabla \cdot \tilde{\mathbf{J}}_\perp$.

It is useful to examine the limiting cases of Eq. (22a). Recall that fluid theory is valid when $k_\perp^2 \lambda_0^2 << 1$, and the collisional limit $\nu_0 / \omega >> 1$ has already been assumed in writing a specific form of the viscosity in Eq. (5). Thus, the magnitude of $\alpha$ is given by the product of a small term with a large one and is not fixed by our ordering; it depends on plasma and neutral densities and the wave vector (toroidal mode number). If the limit $\alpha << 1$ is taken in the perturbed neutral momentum equation, the viscous term is negligible compared with the inertial term, and the neutral pressure gradient term can be neglected compared with the neutral friction term in the perturbed Eq. (5). This means that $k_\perp^2 D_0 << \tilde{\omega}_0$ in $\Lambda$ and $\Upsilon \to 1$ in Eq. (22a). In the opposite limit ($\alpha >> 1$) both the perturbed viscosity and pressure terms are important; in fact, the perturbed pressure term causes $\Upsilon$ to be large, so that terms in square brackets in Eq. (22a) can be neglected in agreement with the corresponding kinetic result of Ref. 1.

The "magnetic line bending" term in the ballooning equation is given by $\nabla \cdot \tilde{\mathbf{J}}_\parallel$, where $\tilde{\mathbf{J}}_\parallel = (c/4\pi)\, k_\perp^2\, \tilde{\mathbf{A}}_\parallel$. In the present ordering Ohm's Law, Eq. (6), reduces simply to the MHD constraint $\tilde{\mathbf{E}}_\parallel = \eta\, \tilde{\mathbf{J}}_\parallel$, which requires that $(\omega + \omega_\eta)\, (i\, \tilde{\mathbf{A}}_\parallel / c) = \boldsymbol{\nabla}_\parallel \tilde{\phi}$, where we

have defined $\omega_\eta = i\,\eta\,k_\perp^2 c^2/4\pi$. Thus, the line-bending term in the ballooning equation is given by

$$\nabla \cdot \tilde{\mathbf{J}}_\parallel = -\frac{ic^2 B}{4\pi\omega}\boldsymbol{\nabla}_\parallel \frac{k_\perp^2}{B}\frac{\omega}{\omega+\omega_\eta}\boldsymbol{\nabla}_\parallel \tilde{\phi} \ . \tag{23}$$

The ballooning equation is obtained by combining Eqs. (20), (22) and (23). Making the nonessential but simplifying assumptions that $\mathbf{k}\cdot\mathbf{u} << \omega$ and $\boldsymbol{\nabla}_\parallel B \approx 0$, and retaining neutral perturbation terms ($\Lambda \neq 0$) with $\alpha >> 1$, the ballooning equation becomes

$$\boldsymbol{\nabla}_\parallel k_\perp^2 \frac{\omega}{\omega+\omega_\eta}\boldsymbol{\nabla}_\parallel \tilde{\phi} + \frac{k_\perp^2}{v_a^2}\left[\omega^2 + \gamma_\kappa^2 + (1-\Lambda)(i\nu\omega + \gamma_\nu^2)\right]\tilde{\phi} = 0 \ , \tag{24a}$$

which agrees with the kinetic result [Eq. (106)] of Ref. 1 when the collisional fluid limit ($\omega,\ k_\perp^2 D_0 << \nu_0$) is taken. This equation is to be solved subject to the usual sheath boundary condition[6,7] of matching the $\tilde{\mathbf{J}}_\parallel$ of the MHD perturbation to the perturbed sheath current:

$$\boldsymbol{\nabla}_\parallel \ln\tilde{\phi} = \frac{-i\,\omega\,\sigma_\theta\,c_s}{k_\perp^2 v_a^2 \rho_s^2} \ , \tag{24b}$$

where $c_s = (T_e/m_i)^{1/2}$ is the ion sound speed, $\rho_s = c_s/\Omega_i$, and $\sigma_\theta = \mathbf{b}\cdot\mathbf{n}/|\mathbf{b}\cdot\mathbf{n}| = \pm 1$ with $\mathbf{n}$ defined as the unit vector normal to the plates and pointing towards the plasma (not to be confused with the toroidal mode number n introduced subsequently). The effect of neutral collisions on the sheath currents is not included in Eq. (24b). A treatment of the effect of ionization in the sheath region on conducting-wall (sheath-driven) modes was given in Ref. 7.

In Eq. (24a), there is a competition between two neutral effects: a stabilizing damping and the potentially destabilizing ion-neutral drag instability. Near the X-point there is a rapid poloidal variation of the components of $\mathbf{k}$ and the equilibrium profiles, which produces oscillations in sign of the drive term $\gamma_\kappa^2 + \gamma_\nu^2$ along the field line, so that the stability problem is potentially very sensitive to the details of the equilibrium. This

motivates the numerical work in Sec. IV. In passing, we note also that Eq. (24) does not contain the sheath instability (i.e. conducting wall modes[6,7]) because for simplicity the analysis here has not retained an equilibrium electric field or temperature perturbations.

To understand the effect of neutral viscosity on ballooning modes, we observe that the neutral terms in the ballooning equation (24) are proportional to

$$1 - \Lambda = \frac{\tilde{\omega}_0 + i\, k_\perp^2\, D_0}{i\nu_0 + \tilde{\omega}_0 + i\, k_\perp^2\, D_0} \tag{25a}$$

$$\approx \frac{\frac{1}{2} k_\perp^2\, \lambda_0^2}{1 + \frac{1}{2} k_\perp^2\, \lambda_0^2}, \qquad (\alpha >> 1) \tag{25b}$$

where the small inertial contribution was neglected for $\alpha >> 1$. This result shows that the effect of ion-neutral friction on ballooning modes is negligible when both the plasma inertia and neutral viscosity are small compared to the collisional damping. In this limit the neutral perturbations "wash out" the effect of the neutrals because the neutrals are carried with the plasma, eliminating the frictional forces that cause damping and instability. The effect of neutral viscosity is to make the neutrals more "rigid" and to increase the strength of the neutral effects.[1]

The scope of the remainder of this paper will be restricted to the unperturbed-neutral limit ($\Lambda \to 0$) in which the neutral physics has the maximum effect on the ballooning stability, although this limit is not justified in all cases. The validity of this approximation will be discussed in Sec. V.

## III. Tokamak Equilibrium Model

### A. Magnetic Geometry

The B-field representation used here is identical to that of Ref. 6 and the reader is referred to the earlier paper for additional details. The magnetic field is expressed in toroidal flux coordinates ($\Psi$, $\chi$, $\phi$ ) as

$$\mathbf{B} = B_\phi \, \mathbf{e}_\phi \; + \; \frac{1}{R} \; \mathbf{e}_\phi \times \nabla\Psi, \tag{26}$$

where $\Psi$ is a poloidal flux function, $\chi$ is an angle-like coordinate in the poloidal direction, $\phi$ is the toroidal angle with $\mathbf{e}_\phi$ the corresponding unit vector, and R is the major radius of the tokamak. The Jacobian of the transformation to flux coordinates is specified by $|\nabla\Psi| = |\nabla\chi| = RB_p$ (where $B_p$ is the poloidal magnetic field), and one then obtains the following projection of the eikonal wavevector in these coordinates:

$$\mathbf{k}_\perp/n = -\frac{1}{|\nabla\Psi|^2}\,\mathbf{B}\times\nabla\Psi + \; (\beta_k - \beta_{ko})\;\nabla\Psi \tag{27}$$

In Eq. (27), n is the toroidal mode number, $\beta_{ko}$ is an integration constant, and the function $\beta_k(\chi)$ is determined by an integration along the field lines:

$$\nabla_\parallel \beta_k = \frac{2}{R\,B_p}\frac{\partial B_p}{\partial \Psi} \; . \tag{28}$$

In the numerical implementation of Eqs. (26) - (28), we employ a "two-wire" model,[6] in which the poloidal magnetic field is represented as the vacuum field obtained from two linear current-carrying filaments. Selected flux surfaces are shown in Fig. 1 for the magnetic field geometry used in this paper; the parameters have been chosen to give a representative single-null X-point equilibrium. For the numerical calculations the flux coordinates are rescaled, $(\Psi, \chi) \rightarrow (\psi,\theta)$, in such a way that the coordinate $\theta$ is a true angle. The X-point is located at $\theta = 0$ (outboard) and $2\pi$ (inboard), and the outer and inner divertor plates are located at $\theta_1 = -\delta$ and $\theta_2 = 2\pi + \delta$, respectively, with $\delta = 0.17$. The symmetry plane, equidistant from both plates, is located at the top of the torus ($\theta = \pi$). The field line curvature $\boldsymbol{\kappa} \equiv \mathbf{b}\cdot\nabla\mathbf{b} = \kappa_\psi \, \mathbf{e}_\psi + \kappa_\theta \, \mathbf{e}_\theta$ with $\mathbf{b} = \mathbf{B} / B$ is calculated in the usual way from Eq. (26) to obtain the MHD ballooning mode instability drive.

The function $\beta_k(\theta)$ is determined by integrating Eq. (28) from $\theta = \theta_1$ to $\theta_2$ (plate to plate) with the integration constant $\beta_{ko} = \beta_k(\theta_o)$ defined such that $k_\psi$ vanishes at the point $\theta = \theta_o$. Here, $\theta_o$ is regarded as the parameter which determines the orientation of $\mathbf{k}_\perp$. It can be shown numerically that $\mathbf{k}_\perp \propto 1/B_p$ and the ratio $k_\psi/k_\theta$ are rapidly varying functions of $\theta$ near the X-points for any value of $\theta_o$ [see Fig. 5 of Ref. 6]. The singular behavior of $\mathbf{k}_\perp$ near the X-point has important consequences for the stability analysis, because it gives a large weighting to the divertor region, thereby enhancing the effect of both the neutral physics and resistivity on MHD modes.

The ballooning equation (24a) and sheath boundary condition (24b) are transformed into the $(\psi, \theta)$ coordinates and the following useful identity is obtained, valid for any scalar function $Q(\psi, \theta)$,

$$\frac{1}{n}\,\mathbf{k}_\perp \cdot \mathbf{b} \times \nabla Q \;=\; -\frac{1}{RC_\perp}\left[\, B\,\frac{\partial Q}{\partial \psi} + (\beta_k - \beta_{ko})\, R^2\, B_p^2\,\frac{\partial Q}{\partial \theta}\,\right] \quad . \tag{29}$$

where $C_\perp$ is defined by $|\nabla\psi| = |\nabla\theta| = B_p/C_\perp$. Finally, the field-line average $\langle Q \rangle$ in Eq. (1), obtained by integrating Eq. (24) along the field line, takes the following form in these coordinates:

$$\langle Q \rangle \;=\; \frac{\int ds\; \tilde{\phi}^2\,(k_\perp^2 / v_a^2)\; Q}{\int ds\; \tilde{\phi}^2\,(k_\perp^2 / v_a^2)} \;=\; \frac{\int d\theta\; \tilde{\phi}^2\,(k_\perp^2 / B_p^2\, v_a^2)\; Q}{\int d\theta\; \tilde{\phi}^2\,(k_\perp^2 / B_p^2\, v_a^2)}\,, \tag{30}$$

where $\nabla_\parallel \equiv \partial/\partial s$ defines the arclength.

If one applies Eq. (29) to the definitions of $\gamma_\kappa^2$ and $\gamma_\nu^2$ in Eq. (1), it is easily seen that the drive terms for the curvature and neutral drag instabilities are sensitive to several aspects of the model: (1) the magnetic shear introduced by the X-point [which determines the function $\beta_k(\theta)$ in the solution to Eq. (28)] ; (2) the choice of $\theta_o$, which determines $\beta_{ko}$; and (3) the plasma and neutral density and pressure profiles [symbolically, $\Lambda(\psi,\theta)$ in Eq. (29)]. These dependences will be studied numerically in Sec. IV. In the next section, we describe the analytic plasma and neutral profiles used in the stability calculations.

**B. Plasma and Neutral Profiles**

In the present work, we use analytical profiles for the plasma and neutral densities and temperatures that allow a reasonable, although not completely self-consistent, description of the attached and detached divertor regimes of operation. The use of model profiles makes possible a more complete survey of parameter space than would be possible with numerically-computed equilibria. We have investigated several equilibrium models and the one discussed here is sufficiently general to illustrate the basic physics of ion-neutral interactions. It will be shown that the MHD stability properties of the divertor region depend on the details of the profiles.

The plasma and neutral profiles are assumed to have the following forms:

$$p_t = \bar{p}_t(\theta)\ \exp[-(\psi - \psi_o)/\lambda_p]\ , \tag{31a}$$

$$n_e = n_i = \bar{n}(\theta)\ \exp[-(\psi - \psi_o)/\lambda_n]\ , \tag{31b}$$

$$T_e = T_i = \bar{T}(\theta)\ \exp[-(\psi - \psi_o)/\lambda_t]\ , \tag{31c}$$

$$n_0 = \bar{n}_0(\theta)\ \exp[-(\psi - \psi_o)/\lambda_{n0}(\theta)]\ , \tag{31d}$$

$$T_0 = \text{constant}\ . \tag{31e}$$

Here, $p_t = p + p_0 = (n_e T_e + n_i T_i) + n_0 T_0$ is the total pressure of the plasma and neutral fluids, $n_e$ and $T_e$ are the electron density and temperature, $n_0$ and $T_0$ are the neutral density and temperature, and $1/\lambda_p = 1/\lambda_n + 1/\lambda_t$. For simplicity, we take $n_e = n_i$, $T_e = T_i$ and $T_0$ is assumed constant along the field line. For attached plasmas, the total pressure $p_t$ is constant along the field line, whereas for detached plasmas $p_t$ is assumed to decrease near the divertor plates. The profile $\bar{n}_0(\theta)$ is chosen to give an exponential decay of the neutral density from its maximum value $n_{0d}$ at the divertor plates to a residual value $n_{0u}$ upstream at the SOL symmetry plane ($\theta = \pi$). The scale length $L_\theta$ of $\bar{n}_0(\theta)$ is chosen to be shorter in the recombination-dominated (detached) plasma than in the high-recycling (attached) plasma, appropriate to the different sources of neutrals in the two cases. $\bar{T}(\theta)$

is specified to give a decrease of $T_e$ from the upstream value $T_{eu}$ to the value $T_{ed}$ at the divertor plates. The density variation $\tilde{n}(\theta)$ along the field line is obtained numerically by solving

$$n_i(\psi,\theta) = n_e(\psi,\theta) = \frac{p_t(\psi,\theta) - n_0(\psi,\theta)\, T_0}{2T_e} . \qquad (32)$$

along the field line. In the attached case, where $p_t(\theta)$ = const., Eq. (32) corresponds to the parallel pressure balance constraint. The physical motivation for Eq. (32) in the detached case will be discussed subsequently.

The radial scale lengths $\lambda_n$ and $\lambda_t$ are assumed to be equal and constant in $\theta$, for simplicity, and positive to ensure radial decay of the plasma pressure, density and temperature away from the separatrix. The variation along the field line of the radial scale length, $\lambda_{n0}(\theta)$, is required to model the complicated $T_e$ dependence of the ion-neutral physics. For detached plasmas, there is a region near the divertor plates where $T_e < 5$ eV and recombination processes dominate.[9] In this region, the neutral density is largest just outside the separatrix, which is modeled here by taking $\lambda_{n0} > 0$. Farther upstream where $T_e > 5$ eV (or for attached plasmas, where this condition is fulfilled everywhere), the neutral density is determined by a balance between recycling and ionization; in this regime $n_0$ peaks radially near the walls, which is modeled by taking $\lambda_{n0} < 0$. The function $\lambda_{n0}(\theta)$ is chosen to give a smooth transition between these two regions. The parameters $\lambda_n$, $\lambda_t$, and those determining $\lambda_{n0}(\theta)$ are held fixed for all the calculations reported here.

Figure 2 shows the variation of $n_i$, $n_0$, and $T_e$ along the field line for two reference equilibria: an "attached, high-recycling" case ($T_{ed}$ = 10 eV, $p_{td}/p_{tu}$ = 1.0, $T_0$ = 1 eV, $p_{0d}/p_{tu}$ = 0.05) and a "detached" case ($T_{ed}$ = 1 eV, $p_{td}/p_{tu}$ = 0.07, $T_0$ = 1 eV, and $p_{0d}/p_{tu}$ = 0.05). The upstream parameters have the following values for both equilibria: $n_{eu} = 1.1 \times 10^{13}$ cm$^{-3}$, $T_{eu}$ = 50 eV, $T_0$ = 1 eV, and $p_{0u}/p_{tu}$ = 0.001. The value of $p_{0d}$, the neutral pressure at the plates, was chosen to make the neutral density approximately equal to the

ion density at the plates in the high-recycling case; note that the neutral contribution to the total pressure is small in all cases considered here. Several qualitative features of these equilibria are important for understanding the sign of the ion-neutral stability terms discussed in Sec. IV. There is a small recombination region ($T_e < 5$ eV) for the detached case [Fig. 2 (b)], whereas $T_e > 5$ eV everywhere for the high-recycling case [Fig. 2 (a)]. In the attached plasma equilbrium, $n_i$ increases near the plates to maintain constant total pressure as $T_e$ decreases, but both $n_i$ and $T_e$ drop near the plates for the detached plasma. Note that the latter equilibrium shows a partial detachment of particles ($n_i$) and a greater degree of detachment of energy ($T_e$) and total pressure (p). The "missing" pressure in the real divertor is absorbed by the walls and dissipated by neutral viscosity, which is outside the scope of the present simplified fluid model and is qualitatively described by making the total pressure $p_t(\theta)$ in Eq. (32) decrease in the vicinity of the divertor plates.

## IV. Numerical Stability Results

An extensive survey of parameter space has been carried out to determine the MHD stability properties of the equilibria described in Sec. III. In this section, we will show that ion-neutral interactions tend to be *stabilizing* for ballooning-interchange modes. The ion-neutral drag instability driven by $\gamma_v^2$ is found in only a small part of parameter space and only for resistive eigenmodes that are highly localized near the plates.

For each equilibrium shown in Fig. 2, we have studied the dependence of the growth rate on the neutral and total pressure at the plates, $p_{0d}$ and $p_{td}$, which are parameterized here by the ratios $\delta_{p0} = p_{0d}/p_{tu}$ and $\delta_{pt} = p_{td}/p_{tu}$; the electron temperature $T_{ed}$ at the plate; the toroidal mode number n; and the parameter $\theta_o$, which determines the orientation of the wavevector **k**. The calculations were done with and without the effects of resistivity [the $\omega_\eta$ term in Eq. (24)], contrasting ideal and resistive ballooning theory.

For the resistive calculations, the product of the effective charge state and the Coulomb logarithm was taken to be $Z_{eff}\ln\Lambda = 26$. Finally, the stability calculations were carried out on two reference field lines in the SOL ($\psi = 0.01$ and 0.03, where $\psi = 0$ is the separatrix); in physical terms, these field lines are located respectively one and three radial scale lengths outside the separatrix.

A summary of the calculations for toroidal mode number n = 100 is given in Tables I and II. Shown in Table I are the growth rates $\gamma = \mathrm{Im}(\omega)$ in units of $10^3\ s^{-1}$ for the most unstable mode after maximizing over $\theta_o$. The first conclusion to be drawn from Table I is that the stability properties of the two reference field lines are quite similar, and in the remainder of this section we will discuss only the innermost field line ($\psi = 0.01$). On each field line, the growth rates are similar for the high-recycling and detached equilibria. This is somewhat fortuitous in the ideal MHD limit; it happens that the sum of the two neutral terms, $i\langle\nu\rangle\omega + \langle\gamma_\nu^2\rangle$, is nearly the same for the two cases, even though the relative size of the neutral terms are quite different [see Table II]. The important point is that the combined effect of the ion-neutral interactions is stabilizing for both equilibria. Finally, Table I shows that resistive ballooning modes are much more unstable than ideal ones for these X-point equilibria. The reason is that the solution of Eq. (27) generates a large $\mathbf{k}_\perp$ near the X-point for the most unstable $\theta_o$.[6] The singularity in $\mathbf{k}_\perp$ produces a large value of $\omega_\eta \propto \eta\ k_\perp^2$, and thus allows the resistive ballooning mode to avoid the neutrals in the divertor region without being stabilized by the magnetic line-bending energy.

This behavior is illustrated in Fig. 3, which shows the eigenfunctions $\tilde{\phi}(\theta)$ of the most unstable ideal and resistive ballooning modes for the the high-recycling equilibrium ($\psi = 0.01$). The ideal mode has the usual ballooning character, being larger in the unfavorable curvature region ($\theta < \pi$), and is finite in the outboard divertor region. (The small depression near the outboard divertor plate at $\theta = -0.17$ is caused by the stabilizing

effect of the neutrals.) The resistive eigenmode is more strongly localized in the unfavorable curvature region and vanishes in both divertor regions; thus, this mode maximizes the curvature drive and avoids both the line-tying effect of the divertor plates (negligible for high n, but substantial for low n) and the stabilizing effect of the ion-neutral collisions. From Table II we note that the most unstable ideal eigenmode has $\theta_o$ = 3.6, whereas the most unstable resistive mode has $\theta_o = 1.5$, indicative of its greater localization on the outboard side. For the detached equilibrium, the most unstable ideal mode (not shown) has $\theta_o = 6.3$ and is interchange-like, $\tilde{\phi}(\theta) \approx$ constant; the resistive eigenfunction for this case is similar to the one shown in Fig. 3. Thus, for both equilibria the combination of X-point geometry and a modest value of resistivity allows the most unstable resistive ballooning mode to avoid the stabilizing divertor region.

We can understand the mode dynamics in more detail by evaluating the integrals in the dispersion relation, Eq. (1), using the eigenfunctions corresponding to Table I. The most important terms are given in Table II, normalized to the curvature drive. The neutral terms are stabilizing for all cases studied, and the instability drive is due to the curvature alone. Comparing the ideal and resistive solutions for the same equilibrium, we see that the line-bending penalty $\langle f_\eta\, k_\parallel^2\, v_a^2 \rangle$ incurred by the resistive eigenfunction in avoiding the divertor is smaller than the decrease in the stabilizing neutral terms. More important, the increased line-bending energy is also compensated by a much larger increase in the curvature drive $\langle \gamma_\kappa^2 \rangle$ due to the mode localization in unfavorable curvature region. Because of these two effects, the resistive growth rate is an order of magnitude larger than the ideal one. In the ideal MHD limit, the neutral friction term $i\langle \nu \rangle \omega$ is much larger than the line bending term; the (stabilizing) ion-neutral drag term $\langle \gamma_\nu^2 \rangle$ is unimportant for the high-recycling case but is comparable to the neutral friction term for the detached case.

To understand the influence of the equilibrium profiles and magnetic geometry on the ion-neutral drag instability, it is useful to write out the geometric dependence of $\gamma_\nu^2$ as follows:

$$\gamma_\nu^2 = \frac{1}{\rho\, k_\perp^2}\, \mathbf{k}\times\mathbf{b}\cdot\nabla \ln\rho \;\; \mathbf{k}\times\mathbf{b}\cdot\nabla p_0 \,,$$

$$\propto \; (k_\theta \frac{\partial n_i}{\partial\psi} - k_\psi \frac{\partial n_i}{\partial\theta})\,(k_\theta \frac{\partial p_0}{\partial\psi} - k_\psi \frac{\partial p_0}{\partial\theta}) \;,$$

$$\approx \; k_\theta^2 \frac{\partial n_i}{\partial\psi}\frac{\partial p_0}{\partial\psi} + k_\psi^2 \frac{\partial n_i}{\partial\theta}\frac{\partial p_0}{\partial\theta} \;\equiv\; T_{\psi\psi} + T_{\theta\theta} \;, \qquad (33)$$

where the last line follows from the numerical observation that in most of the cases studied here the sum of the off-diagonal terms were smaller than the sum of the diagonal terms, $T_{\psi\psi} + T_{\theta\theta}$. Although all terms are retained in the numerical calculations, it is useful for purposes of discussion to make this approximation. For the *high-recycling* equilibrium in Fig. 2 (a), the two terms have opposite signs ($T_{\psi\psi} < 0,\ T_{\theta\theta} > 0$) and tend to cancel, so that $\langle\gamma_\nu^2\rangle$ makes a negligible contribution in this case. More generally, the function $T_{\theta\theta}(\theta)$ is highly localized near the plates whereas $T_{\psi\psi}(\theta)$ is less localized, so that the latter stabilizing effect would be expected to dominate. Moreover, even if we had set $\lambda_n \to \infty$, implying $T_{\psi\psi} = 0$ and $\langle\gamma_\nu^2\rangle > 0$, the sum of the neutral terms $\langle\gamma_\nu^2\rangle + i\langle\nu\rangle\omega$ is negative (stabilizing) for the ideal high-recycling case shown in Table II. In this case it is difficult to arrange a net destabilizing neutral contribution. For the *detached* equilibrium in Fig. 2 (b), the dependence is also complicated: $T_{\psi\psi}$ is positive in the small recombination region and negative in the much larger ionization region, but the line-average of $T_{\psi\psi}$ is negative and therefore stabilizing. Thus, a small region near the plate dominated by recombination physics is not sufficient to drive spatially-extended ballooning modes unstable via the ion-neutral drag mechanism. The $T_{\theta\theta}$ term is also stabilizing for the detached equilibrium, because the gradients along the field line of $n_i$ and $p_0$ are in the opposite direction near the plate. To summarize this discussion, for the

two cases shown in Fig. 2 we find that $\langle\gamma_v^2\rangle < 0$ and the ion-neutral drag term contributes to stabilization of spatially-extended (interchange-ballooning) modes for typical parameters. The stabilization is enhanced by the additional ion-neutral dissipation term, $i\langle\nu\rangle\omega$. The possibility of spatially-localized modes will be discussed subsequently.

The stabilizing effect of the ion-neutral collision terms, $i\langle\nu\rangle\omega + \langle\gamma_v^2\rangle$, increases with neutral pressure as shown in Fig. 4, where we plot the growth rate $\gamma(10^3\,s^{-1})$ versus the parameter $\delta_{p0} = p_{0d}/p_{tu}$ for the high-recycling equilibrium ($\psi = 0.01$). Figure 4 shows that the growth rate drops monotonically with $\delta_{p0}$ over the range shown for both ideal and resistive modes, although the effect is weak in the latter case. The upper limit of $\delta_{p0} = 0.05$ corresponds to the condition that $n_{0d} \le n_{id}$ in the high-recycling case used here. A similar dependence of $\gamma$ on $\delta_{p0}$ is obtained for the detached case (not shown).

The dependence of the growth rate $\gamma$ of spatially-extended ballooning modes on $T_{ed}$ comes about through two equilibrium effects: (1) the pressure weighting of the curvature in the divertor region (a small effect); and (2) the dependence of $n_{id}$, and therefore $\partial n_i/\partial\theta$, on $T_{ed}$ through the pressure balance constraint, Eq.(32). These effects are negligible for resistive ballooning modes, which entirely avoid the divertor region. For ideal modes, there is a dependence of $\gamma$ on $T_{ed}$ only when the $\langle\gamma_v^2\rangle$ term makes a significant contribution to the dispersion relation. Thus, the detached equilibrium is much more sensitive to $T_{ed}$ than the high-recycling one (see Table II).

A plot of the growth rate $\gamma(10^3\,s^{-1})$ of the most unstable ideal mode versus $T_{ed}$(eV) is shown in Fig. 5 with all other parameters the same as in Fig. 2 (b). For these parameters, the most unstable ideal eigenfunction (obtained for $\theta_o = 6.3$) is nearly interchange-like. The total pressure and temperature are detached from the divertor plates ($p_{td}/p_{tu} << 1$, $T_{ed}/T_{eu} << 1$) for the range of $T_{ed}$ shown in Fig. 5. However, the density at the plates is a sensitive function of $T_{ed}$. For $T_{ed} < 0.6$ eV, $n_{id}$ is larger than the upstream

density, so that $\partial n_i/\partial\theta < 0$ near the plates and $\langle\gamma_v^2\rangle > 0$, driven by the $\theta$ dependence of $n_i$ and $p_0$. Thus, the sharp increase in $\gamma$ as $T_{ed} \rightarrow 0$ ($n_{id} \rightarrow \infty$) is due to the ion-neutral drag instability. For example, at $T_{ed} = 0.1$ eV, the line-averaged ion-neutral drag term $\langle\gamma_v^2\rangle$ is more than twice as large as the line-averaged curvature term $\langle\gamma_\kappa^2\rangle$. For $T_{ed} > 0.7$ eV, $n_{id}$ is smaller than the upstream density, with the result that $\partial n_i/\partial\theta > 0$ near the plates and $\langle\gamma_v^2\rangle < 0$. Thus, in this parameter regime $\langle\gamma_v^2\rangle$ is stabilizing and accounts for the decrease in $\gamma$ with $T_{ed}$. Figure 5 shows that the ideal mode is completely stabilized by this effect for $T_{ed} > 1.8$ eV when resistivity is neglected.

This discussion has one caveat. It is doubtful whether the equilibrium behavior for $T_{ed} < 0.6$ eV (i.e. the ion density rise near the plates) is compatible with the physics of recombination (except possibly when an ionizing energetic electron tail is also present), but it is included in Fig. 5 to demonstrate that our ballooning code can find the ion-neutral drag instability when the dominant gradients of $n_i$ and $p_0$ are in the same direction.

We return now to the important role of resistivity in determining SOL stability in the presence of neutrals. The competition between the effects of resistivity and ion-neutral collisions is shown in Fig. 6 as a function of toroidal mode number n. Here, we have plotted the ballooning growth rate $\gamma(10^3\ s^{-1})$ versus n for four stability models: (a) resistive ballooning without neutrals ($\delta_{p0} = 0$), (b) resistive ballooning with neutrals, (c) ideal ballooning without neutrals, and (d) ideal ballooning with neutrals. In each case, the high-recycling equilibrium was used with $\psi = 0.01$ and the most unstable $\theta_o$ for n = 100 (see Table II). Comparing curves (a) and (b), we find that the relative change in the resistive growth rate due to neutrals is weak for $n > 50$. At very low mode numbers ($n < 20$) the resistive modes become ideal and consequently are strongly stabilized by a combination of line-tying and ion-neutral collisions. As already discussed, the resistive

eigenmode can avoid the divertor regions when $\omega_\eta >> \omega$, and this condition is more easily satisfied at high n since $\omega_\eta \propto \eta\ k_\perp^2 \propto n^2$. In the ideal MHD limit [curves (c) and (d)], the ion-neutral interactions are strongly stabilizing for all n. The large difference between the resistive and ideal curves in this figure suggest that it is important to use the resistive stability model in doing these calculations.

There are important caveats concerning the mode number dependence shown in Fig. 6. At very low mode number, the eikonal formalism is suspect. In addition, fluid drifts ($\omega_*$ terms) must be retained at intermediate and high n for an accurate quantitative stability analysis, but the present resistive MHD model is sufficient to illustrate our main conceptual points.

We have seen that an extensive search of parameter space yields the conclusion that global SOL ballooning instabilities, extending from one divertor region to the other, are driven unstable mainly by the curvature drive in the present model, where drift and sheath instabilities are not retained. To the extent that neutral collisions matter at all, the effect of ion-neutral friction tends to be stabilizing. The effect of resistivity on these modes is to disconnect them from the divertor regions and reduce the effect of neutrals on the modes.

It is natural to ask whether resistivity can also permit a class of modes which are driven unstable by the *ion-neutral drag* mechanism and are localized in the *divertor* region. We have obtained such solutions numerically for the low temperature detached equilibria ($T_{ed} < 0.6$ eV) discussed in Fig. 5. In Fig. 7, the function $\gamma_\nu^2(\theta)/\gamma_{mhd}^2$, where $\gamma_{mhd} = v_i / (R\lambda_n)^{1/2}$ is a typical MHD growth rate, and the corresponding eigenfunction $\tilde{\phi}(\theta)$ are plotted in the outboard divertor region ($-0.17 < \theta < 0$) for the parameters n = 100, $\theta_o = 6.3$, $T_{ed} = 0.1$ eV and $Z_{eff} \ln \Lambda = 0.5$. The growth rate of this mode is substantial ($\gamma = 242$ in the units of Table I). Note that the eigenfunction and instability

drive are confined to the narrow region near the plate where $\partial/\partial\theta$ is largest, and the eigenfunction peaks at the maximum of $\gamma_\nu^2(\theta)$. The width of the eigenfunction is already quite narrow for the artificially small value of resistivity used in this case, and it becomes even narrower as $Z_{eff} \ln \Lambda$ is increased. We remark that here the growth rate for an unstable mode localized in the *outboard* divertor region is maximized by choosing $\theta_o$ near the *inboard* divertor plate ($\theta_o = 6.3$), a behavior very different from a curvature-driven MHD mode. The reason is that this choice of $\theta_o$ makes the ratio of $k_\psi/k_\theta$ large in the outboard divertor region, which in turn increases the ratio of $T_{\theta\theta}/T_{\psi\psi}$ [see Eq. (33)] and therefore the drive term $\gamma_\nu^2$. We conclude that even a small amount of resistivity permits the existence of highly-localized instabilities driven by the ion-neutral drag mechanism, but the conditions for positive $\gamma_\nu^2(\theta)$ are somewhat suspect, as discussed after Fig. 5.

## V. Summary and Discussion

In this paper, we have examined the influence of ion-neutral interactions, such as charge exchange and elastic scattering, on the linear stability of MHD modes in the SOL of tokamak divertor plasmas. The numerical calculations employ the high-n ballooning equation (ideal and resistive), applied to a single-null X-point geometry with specified plasma profiles along and across the magnetic field lines. In addition to standard MHD physics (curvature drive, line bending, line tying, etc.), the ballooning equation, Eq. (24), includes two ion-neutral terms, collisional dissipation [$\omega^2 \rightarrow \omega(\omega + i\nu\omega)$] and the drive term $\gamma_\nu^2$ for the ion-neutral drag instability, in the unperturbed neutral limit ($\Lambda \rightarrow 0$). This instability is well-known in experiments with weakly-ionized plasmas[4,5] and was thought possibly to be relevant to divertor plasmas.[1-3]

The main results of this study are as follows. First, it was shown that the ion-neutral interaction terms can be large for modest neutral pressures ($p_{0d}/p_d << 1$) and densities ($n_{0d}/n_{id} < 1$); the neutral terms tend to be *stabilizing* for typical attached and detached divertor plasmas [see Table II and Fig. 6]. The conditions for obtaining the ion-neutral drag instability are hard to obtain in divertor plasmas when realistic geometry is considered. This point will be discussed further below. Second, our results indicate that the resistive effects are especially important for SOL stability calculations with neutrals in X-point geometry. When resistivity is retained, the magnetic line bending term is reduced sufficiently near the X-points (where $k_\perp \rightarrow \infty$ ) that the most unstable curvature-driven eigenfunction avoids the stabilizing neutral effects in the divertor region. In the resistive limit, the influence of the ion-neutral interactions on the growth rate is small for high n (toroidal mode number). At low n, where the effects of resistivity are small, the ion-neutral physics can be important [Fig. 6], but this limit is not accurately described by our eikonal model.

It is important to understand the physical reason for the absence of the ion-neutral drag instability for most divertor equilibria examined here. The analytic condition for the ion-neutral drag term to be destabilizing ($\gamma_\nu^2 > 0$) is that $\nabla n_i$ have a component parallel to $\nabla p_0$ [see Eq. (33)]. In X-point geometry with the most unstable $\theta_o$, it is found numerically that $k_\psi^2 >> k_\theta^2$ in the region near the divertor plates where the neutral terms are large. (This occurs because $k_\psi$ is driven by the large magnetic shear near the X-point.) Thus, the relevant instability condition is $\nabla_\theta n_i \, \nabla_\theta p_0 > 0$. This condition can be satisfied if $T_e$ decreases sufficiently strongly in the vicinity of the divertor plates ($T_{ed} << T_{eu}$) that the ion density rises, i.e. $n_{id} >> n_{iu}$. However, the *total* effect of the neutrals is destabilizing only if $\gamma_\nu^2$ exceeds the stabilizing collisional dissipation, i.e. $\gamma_\nu^2 - \gamma\nu > 0$,

where $\gamma$ is the growth rate of the mode. This is a quantitative question, which can be answered only by detailed numerical solution of the ballooning equation.

For the equilibria considered here, the detached cases do not satisfy $\nabla_\theta n_i \nabla_\theta p_0 > 0$, and the attached cases with $T_{ed} > 10$ eV fail to achieve $\gamma_\nu^2 > \gamma\nu$. Both conditions were satisfied only for equilibria with very low values of $T_e$ at the plate, so low, in fact, that the plasma would be dominated by recombination near the plates.[9] However, it is not clear that high $n_{id}$ is physically consistent for a recombination-dominated situation, and therefore a discussion of these cases was not emphasized. It was noted in passing that the ion-neutral drag instability was obtained numerically for such equilibria when a small amount of resistivity was used. Both global (near-interchange) eigenfunctions and ones localized entirely in the divertor region [Fig. 7] can be obtained.

In summary, we have found that ion-neutral interactions in the divertor tend to be stabilizing for ideal modes (for the most realistic divertor equilibria) and have little effect on resistive modes, which tend to avoid the divertor regions. For SOL ballooning modes, neutral particle effects should be largest at low toroidal mode numbers, for which a better theory is needed. The possibility of unstable ion-neutral drag modes localized in the divertor has also been demonstrated, but more work is needed to evaluate whether the requirements for these modes are physically realistic.

Finally, we discuss the validity of the unperturbed-neutral ($\Lambda = 0$) fluid model used in the numerical work. Equation (25) shows that the effect of viscosity enhances the validity of the unperturbed-neutral model, but this effect is limited by the validity condition of the fluid equations, $k_\perp^2 \lambda_0^2 < 1$. In fact, it is often difficult to justify fluid theory for either the equilibrium or the stability of typical divertor plasmas, but a kinetic treatment is beyond the scope of this paper. Moreover, the present simple model was used as a means of exploring the important role of X-point geometry for divertor stability

calculations and because the main conclusions derived from it are likely to be independent of this approximation: (i) the result that $\gamma_v^2$ tends to be stabilizing for realistic equilibria is expected to hold in more general models, because it was shown in the kinetic treatment of Ref. 1 that the neutral perturbations reduce the growth rate but do not change the sign of $\gamma$; and (ii) the result that high-n resistive modes tend to avoid the neutral-dominated regions is not strongly affected by the details of the neutral model, as long as the effect of the neutrals is stabilizing. This effect is enhanced by the synergism of X-point geometry and resistivity discussed in our paper.

A useful but difficult extension of the present work would be a low mode number treatment of ion-neutral frictional effects in divertor geometry retaining neutral perturbations in the fully kinetic regime. In the low-n limit, resistivity is not dominant [Fig. 6] and one expects the effects of the ion-neutral friction to be important; the estimates given here and in Ref. 1 indicate that the neutral perturbations should be retained for these modes.

**Acknowledgments**

The authors would like to thank S. Krasheninnikov, P. Catto, O. Batishchev, G. Porter and T. D. Rognlien for several helpful discussions on divertor issues. We also thank the referee for calling our attention to the treatment of viscosity in Ref. 1.

This work was supported by the U.S. Department of Energy (DOE) under Grant No. DE-FG02-97ER54392; however, this support does not constitute an endorsement by the DOE of the views expressed herein.

## References


1. W. Daughton, B. Coppi, P. Catto, and S. Krasheninnikov, Phys. Plasmas **5**, 2217 (1998).
2. D. A. D'Ippolito and J. R. Myra, Bull. Am. Phys. Soc. (Plasma Physics) **42**, 1823 (1997), paper oThaP1-17.
3. D. R. McCarthy, S. P. Tucker, S. I. Krasheninnikov, and P. J. Catto, Contrib. Plasma Phys., **38 1/2**, 201 (1998).
4. A. Simon, Phys. Fluids **6**, 382 (1963).
5. D. A. D'Ippolito and N. A. Krall, Phys. Fluids **17**, 1852 (1974).
6. J. R. Myra, D. A. D'Ippolito, and J. P. Goedbloed, Phys. Plasmas **4**, 1330 (1997).
7. H. L. Berk, D. D. Ryutov, and Yu. A. Tsidulko, Phys. Fluids B **3,** 1346 (1991).
8. X. Q. Xu and R. H. Cohen, Plasma Phys. Cont. Fusion **35**, 1071 (1993).
9. S. I. Krasheninnikov, A. Yu. Pigarov, D. A. Knoll, B. LaBombard, B. Lipschultz, D. J. Sigmar, T. K. Soboleva, J. L. Terry, and F. Wising, Phys. Plasmas **4**, 1638 (1997).

TABLE I. Growth rates in units of $10^3$ $s^{-1}$ of the most unstable eigenmode with n = 100. Results of ideal and resistive ballooning stability calculations are given on two reference field lines in the SOL ($\psi$ = 0.01 and 0.03) for the two equilibria shown in Fig. 2. For comparison, the growth rates without neutrals (in the same units) is 65 in the ideal case and 265 in the resistive case for the high-recycling equilibrium ($\psi$ = 0.01).

| Case | High-Recycling | Detached |
|---|---|---|
| $\psi$ = 0.01, ideal | 12 | 13 |
| $\psi$ = 0.01, resistive | 230 | 240 |
| $\psi$ = 0.03, ideal | 38 | 35 |
| $\psi$ = 0.03, resistive | 235 | 246 |

TABLE II. Values of the ballooning parameter $\theta_o$ and the terms in the dispersion relation, Eq. (1), normalized to the curvature drive for the most unstable eigenmode (with n = 100 and $\psi$ = 0.01). Here, $f_\eta = \omega/(\omega + \omega_\eta)$ is the resistivity factor. The minus signs indicate that the neutral and line bending terms are stabilizing.

| | High-Recycling | | Detached | |
|---|---|---|---|---|
| | ideal | resistive | ideal | resistive |
| $\theta_o$ | 3.6 | 1.5 | 6.3 | 1.5 |
| $\langle f_\eta k_\parallel^2 v_a^2 \rangle / \langle\gamma_\kappa^2\rangle$ | –0.10 | –0.49 | –0.01 | –0.48 |
| $i\langle\nu\rangle\omega / \langle\gamma_\kappa^2\rangle$ | –0.85 | –0.11 | –0.44 | –0.04 |
| $\langle\gamma_\nu^2\rangle / \langle\gamma_\kappa^2\rangle$ | –0.02 | –0.07 | –0.40 | –0.07 |

**Figure Captions**

Fig. 1 Selected flux (constant $\psi$) surfaces near the separatrix for the two-wire model of a single-null X-point divertor. [From Myra et al., Ref. 6]

Fig. 2 Normalized equilibrium profiles $n_i/n_{0d}$ (dashed line), $n_0/n_{0d}$ (solid line), and $T_e/T_{eu}$ (dotted line) versus $\theta$ on the reference field line $\psi = \psi_o$ for two equilibria described in the text: (a) an attached high-recycling case and (b) a detached case. Only the region near the outboard divertor and X point ($-0.17 < \theta < 1.0$) is shown. The normalizations are to upstream (u) and divertor plate (d) values.

Fig. 3 Eigenfunctions $\tilde{\phi}(\theta)$ for n = 100, the most unstable value of $\theta_o$, and the high-recycling equilibrium described in the text. Shown are the ideal ballooning eigenfunction with $\theta_o = 3.6$ (solid line) and the resistive ballooning mode with $\theta_o = 1.5$ (dashed line).

Fig. 4 Growth rate $\gamma\,(10^3\ s^{-1})$ of the most unstable n = 100 mode versus normalized neutral pressure at the divertor plate ($\delta_{p0} = p_{0d}/p_{tu}$) for the field line $\psi = 0.01$ and the high-recycling equilibrium. Shown are the ideal case (solid line) and the resistive case (dashed curve). For each curve, the most unstable value of $\theta_o$ is independent of $\delta_{p0}$ and has the value shown in Table II.

Fig. 5 Growth rate $\gamma\,(10^3\ s^{-1})$ of the most unstable n = 100 ideal mode ($\theta_o = 6.3$) versus $T_{ed}$(eV) for detached equilibria ($p_{td}/p_{tu} << 1$, $T_{ed}/T_{eu} << 1$). The observed variation with temperature is due to the ion-neutral drag term $\langle\gamma_v^2\rangle$. The sharp rise of $\gamma$ as $T_{ed} \to 0$ ($n_{id} \to \infty$) is due to the ion-neutral drag instability. The mode stabilization for $T_{ed} > 1.8$ eV is also caused by $\langle\gamma_v^2\rangle$, which reverses sign for $T_{ed} > 0.7$ eV as explained in the text.

Fig. 6 Growth rate $\gamma\,(10^3\ s^{-1})$ versus toroidal mode number n for the high-recycling equilibrium ($\psi = 0.01$) with several stability models: (a) resistive model without neutrals (dashed line); (b) resistive model with neutrals (solid line); (c) ideal model without neutrals (dashed line); and (d) ideal model with neutrals (solid line). For each curve, the most unstable $\theta_o$ for n = 100 was used (see Table II).

Fig. 7 Plot of the eigenfunction $\tilde{\phi}(\theta)$ (solid line) and the instability drive $\gamma_v^2(\theta)/\gamma_{mhd}^2$ (dashed line) in the outboard divertor region for n = 100, $\theta_o$ = 6.3, and the detached equilibrium with the parameters $T_{ed}$ = 0.1 eV and $Z_{eff}$ ln $\Lambda$ = 0.5. Thus, a small amount of resistivity permits a highly localized branch of the ion-neutral drag instability.

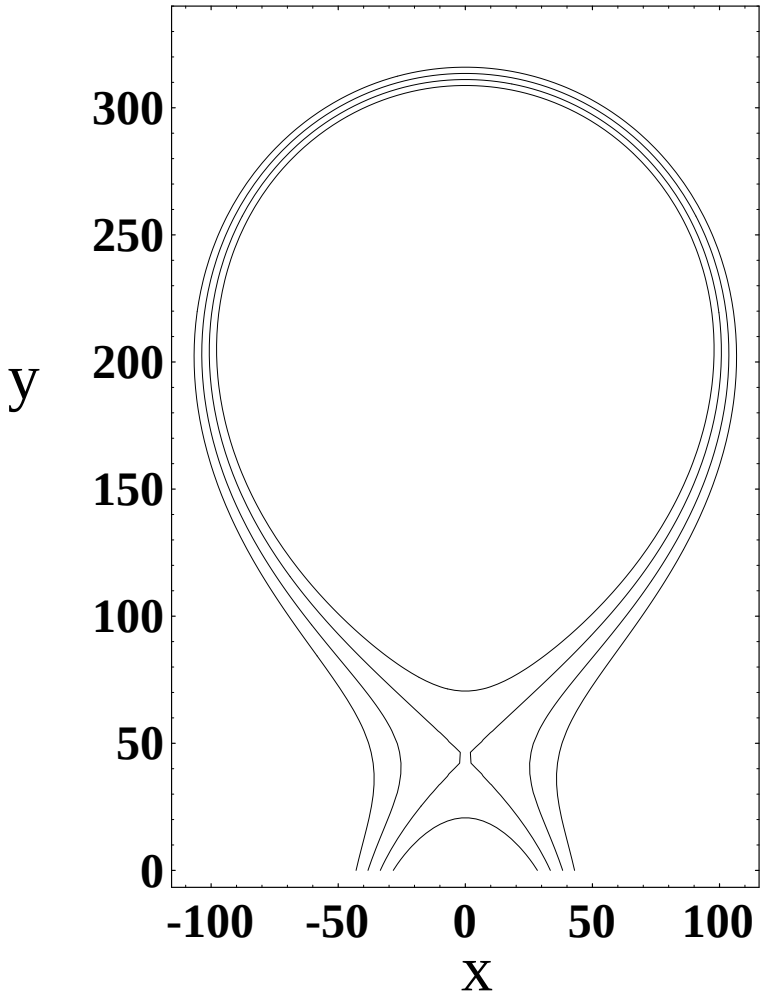


Fig. 1 Selected flux (constant $\psi$ ) surfaces near the separatrix for the two-wire model of a single-null X-point divertor. [From Myra et al., Ref. 6]

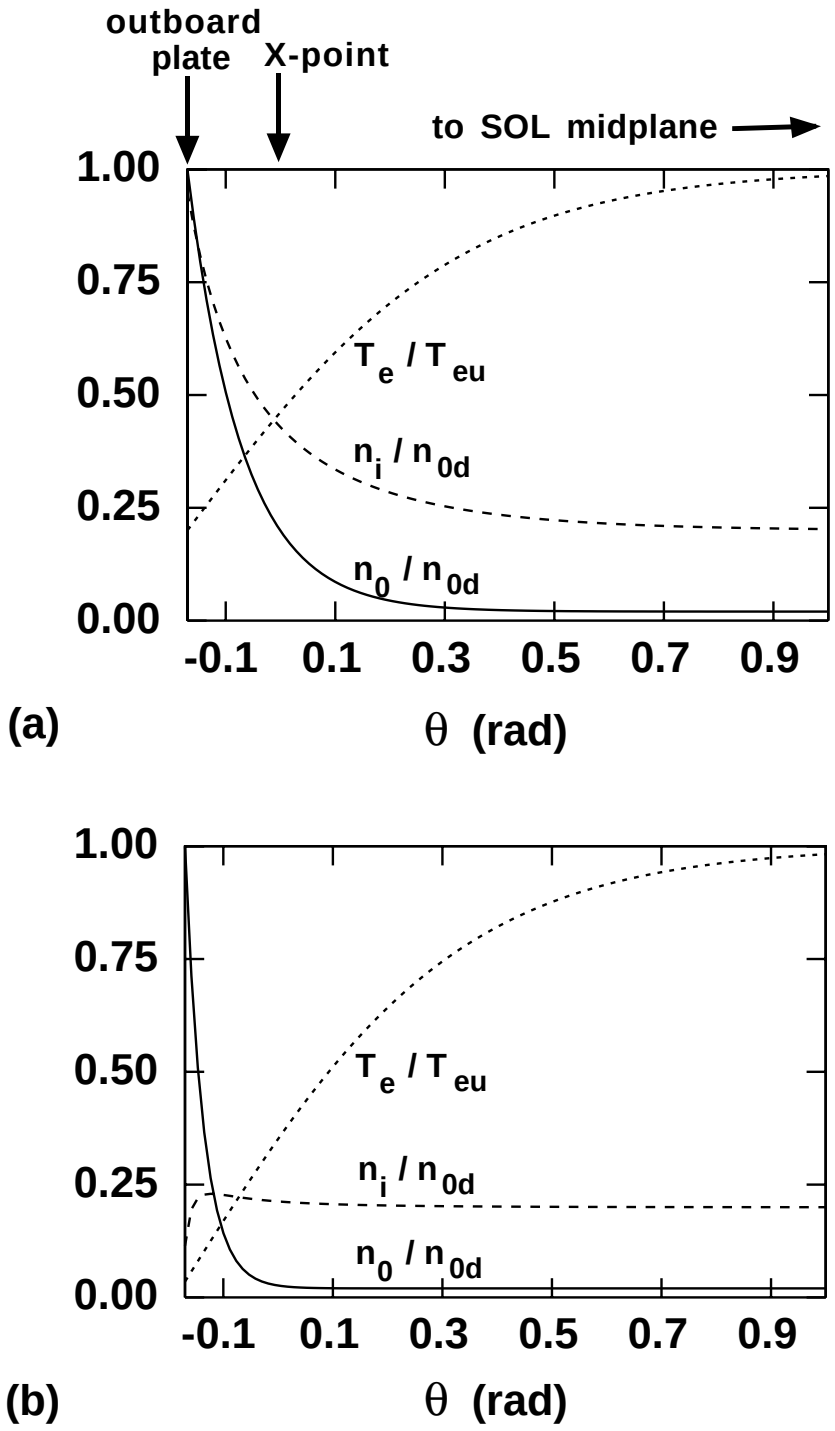


Fig. 2 Normalized equilibrium profiles $n_i/n_{0d}$ (dashed line), $n_0/n_{0d}$ (solid line), and $T_e/T_{eu}$ (dotted line) versus $\theta$ on the reference field line $\psi = \psi_o$ for two equilibria described in the text: (a) an attached high-recycling case and (b) a detached case. Only the region near the outboard divertor and X point ($-0.17 < \theta < 1.0$) is shown. The normalizations are to upstream (u) and divertor plate (d) values.

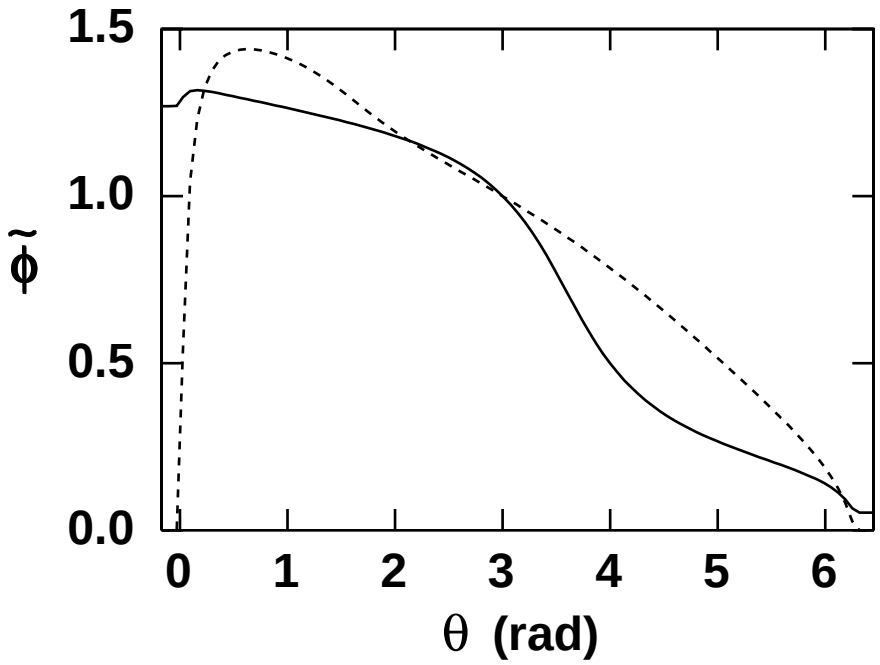


Fig. 3 Eigenfunctions $\tilde{\phi}(\theta)$ for n = 100, the most unstable value of $\theta_o$, and the high-recycling equilibrium described in the text. Shown are the ideal ballooning eigenfunction with $\theta_o$ = 3.6 (solid line) and the resistive ballooning mode with $\theta_o$ = 1.5 (dashed line).

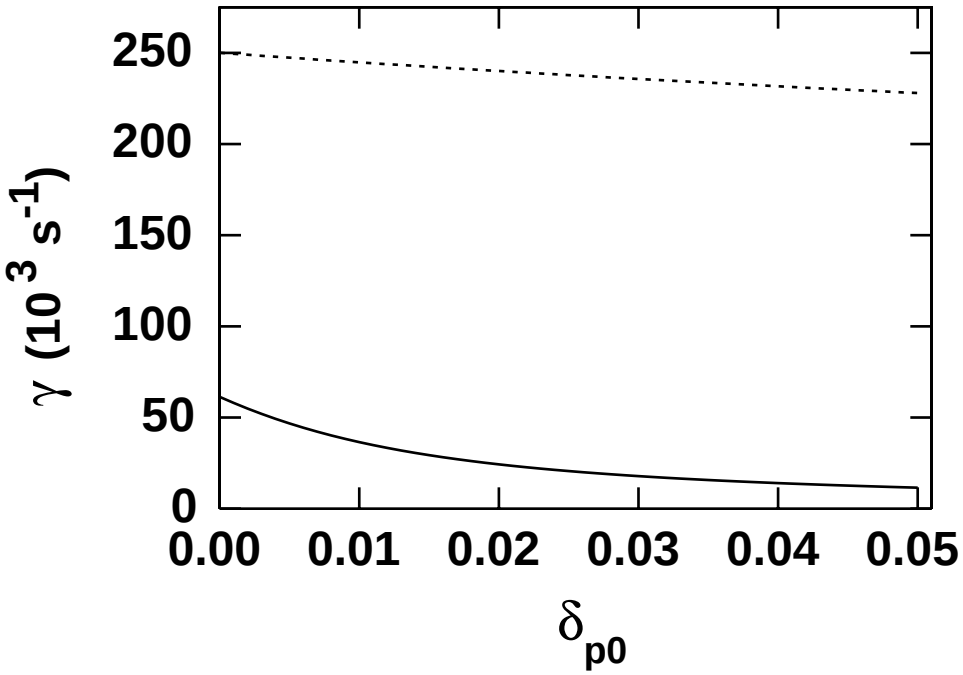


Fig. 4 Growth rate $\gamma$ ($10^3$ $s^{-1}$) of the most unstable n = 100 mode versus normalized neutral pressure at the divertor plate ($\delta_{p0} = p_{0d}/p_{tu}$) for the field line $\psi = 0.01$ and the high-recycling equilibrium. Shown are the ideal case (solid line) and the resistive case (dashed curve). For each curve, the most unstable value of $\theta_o$ is independent of $\delta_{p0}$ and has the value shown in Table II.

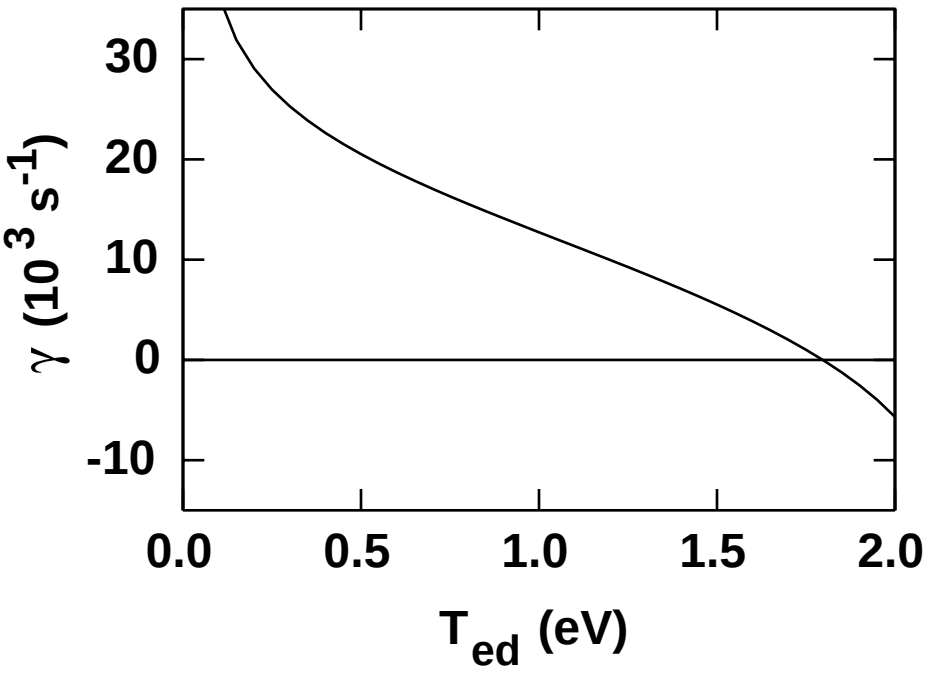


Fig. 5 Growth rate $\gamma$ ($10^3$ $s^{-1}$) of the most unstable n = 100 ideal mode ($\theta_o$ = 6.3) versus $T_{ed}$(eV) for detached equilibria ($p_{td}/p_{tu}$ <<1, $T_{ed}/T_{eu}$ << 1). The observed variation with temperature is due to the ion-neutral drag term $\gamma_\nu^2$. The sharp rise of $\gamma$ as $T_{ed} \rightarrow 0$ ($n_{id} \rightarrow \infty$ ) is due to the ion-neutral drag instability. The mode stabilization for $T_{ed}$ > 1.8 eV is also caused by $\gamma_\nu^2$ , which reverses sign for $T_{ed}$ > 0.7 eV as explained in the text.

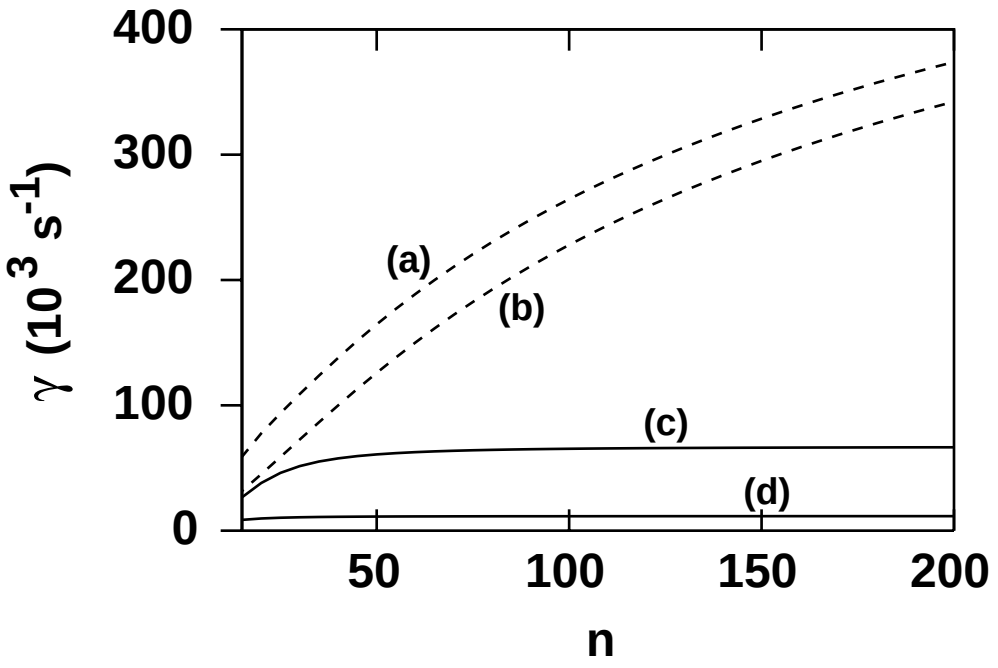


Fig. 6 Growth rate $\gamma$ ($10^3$ $s^{-1}$) versus toroidal mode number n for the high-recycling equilibrium ($\psi$ = 0.01) with several stability models: (a) resistive model without neutrals (dashed line); (b) resistive model with neutrals (solid line); (c) ideal model without neutrals (dashed line); and (d) ideal model with neutrals (solid line). For each curve, the most unstable $\theta_o$ for n = 100 was used (see Table II).

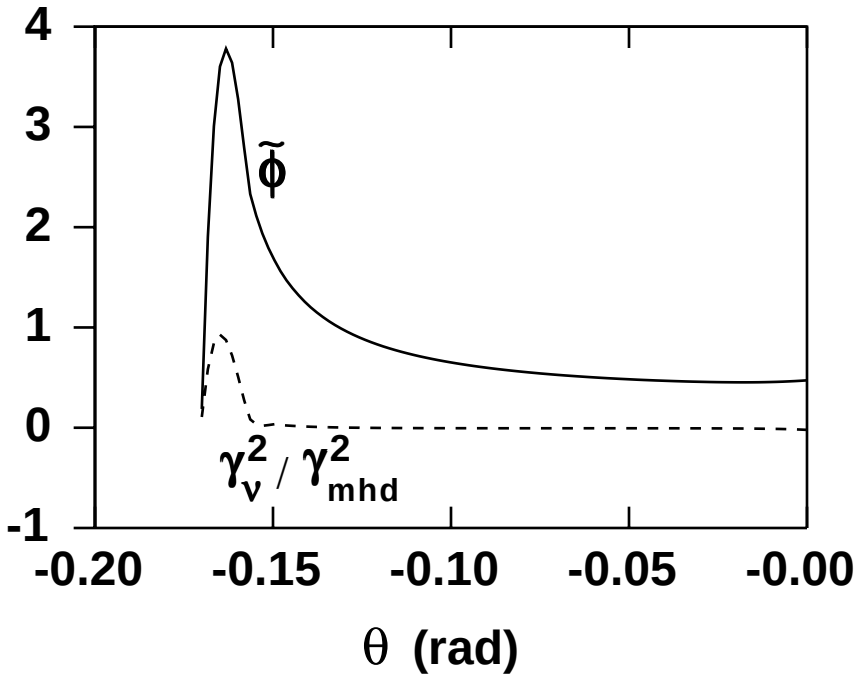


Fig. 7 Plot of the eigenfunction $\tilde{\phi}(\theta)$ (solid line) and the instability drive $\gamma_{v(\theta)}^2 / \gamma_{mhd}^2$ (dashed line) in the outboard divertor region for n = 100, $\theta_o$ = 6.3, and the detached equilibrium with the parameters $T_{ed}$ = 0.1 eV and $Z_{eff}$ ln $\Lambda$ = 0.5. Thus, a small amount of resistivity permits a highly localized branch of the ion-neutral drag instability.